Asian Journal of Chemistry; Vol. 35, No. 8 (2023), 1799-1809

ASIAN JOURNAL OF CHEMISTRY

https://doi.org/10.14233/ajchem.2023.27960

Friedolanostanes from *Garcinia benthamii* Pierre: *in silico* Investigation of Anti-inflammatory Activity Targeting the NF-κB p50 Subunit

JASMINE U. TING[1], CONSOLACION Y. RAGASA[1], ROMEO B. LEROM[2], CHIEN-CHANG SHEN[3], VINCENT ANTONIO S. NG[1], MARIA CARMEN S. TAN[1,*] and GLENN G. OYONG[4,*]

[1]Department of Chemistry, De La Salle University, 2401 Taft Avenue, Manila 1004, Philippines
[2]Natural Sciences Department, College of Arts and Sciences, Western Philippines University, Aborlan, 5302, Philippines
[3]National Research Institute of Chinese Medicine, Ministry of Health and Welfare, 155-1, Li-Nong St., Sec. 2, Taipei, Taiwan
[4]Molecular Science Unit Laboratory, Center for Natural Science and Environmental Research, De La Salle University, 2401 Taft Avenue, Manila 1004, Philippines

*Corresponding authors: Tel/Fax: +63 2 5360230; E-mail: maria.carmen.tan@dlsu.edu.ph; glenn.oyong@dlsu.edu.ph

Received: 9 May 2023; *Accepted*: 3 June 2023; *Published online*: 31 July 2023; AJC-21310

An investigation of the chemical constituents present in the dichloromethane (DCM) extracts of rind, fruit, roots and leaves of *Garcinia benthamii* Pierre has led to an isolation of a new triterpene (24*E*)-23-acetoxy-3α-hydroxylanosta-9(11),16,24-trien-26-oic acid (**1**), squalene and triacylglycerols from the roots; methyl (24*E*)-3α,9α,23-trihydroxy-17,14-friedolanosta-14,24-dien-26-oate (**2**), caryophyllene, squalene, a mixture of compound **1**, (22*Z*,24*E*)-9α-hydroxy-3-oxo-17,14-friedolanosta-14,22,24-trien-26-oic acid (**3**) and another new triterpene (24*E*)-9α-hydroxy-3-oxo-17,14-friedolanosta-14,24-dien-26-oic acid (**4**) derived from pericarp; a combination of compound **3** and the new isolated triterpene methyl (24*E*)-9α,23-dihydroxy-3-oxo-17,14-friedolanosta-14,24-dien-26-oate (**5**), triacylglycerols, friedelin, squalene and a mixture of β-sitosterol and stigmasterol accrued from the outer covering of the stalk; compound **2**, caryophyllene, α-carotene and chlorophyll a originating from the leaves; compound **2** and a blend of β-sitosterol and stigmasterol from the blooms; δ-tocotrienol, squalene and triacylglycerols from the mesocarp; and triacylglycerols and a composite of stigmasterol and β-sitosterol recovered from the seeds of *G. benthamii*. The molecular orientation of compound **1** was characterized by comprehensive 1D and 2D NMR examinations while compounds **2-5** were elucidated by 1D NMR spectroscopy since a new triterpene **4** was observed to have a small difference with compound **3** in C-22 and compound **5** was observed to have a difference with the C-3 signal of compound **2**. To further examine the possible bioactivities of the friedolanostanes especially the new molecules, the anti-inflammatory potential of these compounds was predicted through docking analysis in Autodock Vina. Four of the identified friedolanostanes (**2-5**) were found to have higher binding affinities to NF-κB p50 homodimer than the control dexamethasone. Considering all the probable interactions of 9 amino acid residues, (Arg 57, Tyr 60, Glu 63, Lys 244, Pro 246, Lys 275, Arg 308, Gln 309 and Phe 310) perceivable binding mechanisms were observed to actively interact with the compounds either by conventional hydrogen bonding or by van der Waals forces. Further confirmation from the molecular dynamics study revealed that the stability of the protein-ligand complexes with compounds **2-5** had no significant conformational changes in the structure of the p50 homodimer. Hence, this study provided a chemical profile of the DCM extract obtained from the plant and propose a potential anti-inflammatory activity of the friedolanostanes through *in silico* investigation. Friedolanostanes (**2-5**)with promising anti-inflammatory activity may be synthesized and subjected to *in vitro* and *in vivo* investigation to establish the anti-inflammatory properties.

Keywords: *Garcinia benthamii* Pierre, *Garcinia ferrea* Pierre, Friedolanostanes, Anti-inflammatory, NF-κB p50.

INTRODUCTION

Garcinia benthamii Pierre (syn. *Garcinia ferrea* Pierre), classified under the family Clusiaceae/Guttiferae, is locally called Bunog by the Cuyunin tribe and Tagbanua located in Palawan [1]. It is a tree that can reach 20 m in height, bears white flowers during the months of March and April and bears distinctive small berry fruits [2]. In Aborlan, Palawan, Philippines, the tree is considered as very durable timber, which is highly sought after for house posts [3]. Landscapers have often used

this because of its good canopy. The fruit is edible with sour or acidic taste and has been investigated as a possible starting source for the production of wine, however, much studies must be further achieved since it has not yet been accepted by wine drinkers for its palatability [4].

Earlier reported examinations of *G. benthamii* bark afforded a new benzophenone, salimbenzophenone [5]. Furthermore, the isolation of friedolanostanes, (22*Z*,24*E*)-3β-acetoxy-9α-hydroxy-17,14-friedolanosta-14,22,24-trien-26-oic acid, (22*Z*,24*E*)-3β,9α-dihydroxy-17,14-friedolanosta-14,22,24-trien-26-oic acid, (22*Z*,24*E*)-9α-hydroxy-3-oxo-17,14-friedolanosta-14,22,24-trien-26-oic acid, a friedocycloartane, (22*Z*, 24*E*)-3α-hydroxy-17,13-friedocycloarta-12,22,24-trien-26-oic acid and a benzophenone, benthaphenone, (22*Z*,24*E*)-3α,9α-dihydroxy-17,13-friedolanosta-12,22,24-trien-26-oic acid, methyl (24*E*)-3α,23-dihydroxy-17,14-friedolanosta-8,14,24-trien-26-oate, glutinol, lupeol and stigmasterol from the leaves and bark of *G. benthamii* have been reported [2]. Recently, a study described the isolation of 1,3,6,7-tetrahydroxyxanthone from *G. benthamii* leaves, which exhibited promising antioxidant activity in a DPPH radical scavenging experiment (IC_{50} = 8.01 μg/mL) [6].

The ethanolic extracts of the different parts of *G. ferrea* exhibited moderate anti-HIV-1 protease activity with IC_{50} values of 45.5, 47.6 and 27.3 μg/mL for the root, fruit and stem extracts, respectively [7]. A new protostane, (22*Z*,24*E*)-3-oxoprotosta-12,22,24-trien-26-oic acid, two novel lanostane lactones, garciferolides A and B, along with dulxanthone A, 6-hydroxy-1,5-dimethoxyxanthone and 2-hydroxyxanthone, were obtained from the bark of *G. ferrea* [8].

As observed, most of the identified compounds in *G. benthamii* were predominantly terpenes. Other than the activities mentioned earlier, terpenes are also known to have anti-inflammatory activity [9]. Many of the terpenes have been reported to inhibit the NF-κB signal by diverse mechanisms. One mechanism is through hindering the DNA binding process through affecting the NF-κB subunits [10]. Studies revealed that binding to NF-κB subunits like the p50 homodimer could effectively limit the DNA binding process and subsequent activity of NF-κB through the inhibition of the induction of inflammation by limiting the production of pro-inflammatory cytokines like TNF-α and IL-6 [11]. Many of the triterpenes having the same backbone as friedolanostanes were observed to be effective inhibitors of NF-κB [10,11].

Limited studies have been conducted on the anti-inflammatory ability of friedolanostanes. It is the reason that this study investigated the potential anti-inflammatory activities of friedolanostanes (**2-5**) (Fig. 1) by performing molecular docking analysis *via* Autodock Vina [12]. For the *in silico* study, the FDA-approved anti-inflammatory drug, dexamethasone, served as the positive control. Comparisons of the reported compounds and the control using the pharmacophore descriptors were investigated through PharmaGist [13]. Molecular dynamics trials were performed on these protein-ligand complexes to check for their stability. Lastly, the pharmacokinetics of the compounds were predicted through ADMETlab [14] to determine their drug-likeness and ADMET properties.

EXPERIMENTAL

General isolation procedure: A blender was used to reduce the particle size of air-dried roots (142.4 g), fruit peel (547.3 g), stem bark (160 g), flowers (16.9 g), flesh of the fruit (17.4 g) and seeds (24.0 g) of *G. benthamii.* For extraction process, the plant samples were soaked in CH_2Cl_2 for 3 days and filtered. *In vacuo*, these filtrates were concentrated and 4.5 g of crude extracts from roots, 23.9 g from fruit peel, 1.97 g from stem bark, 0.80 g from flowers, 1.43 g from flesh of fruit and 0.57 g of seeds were obtained. Through column chromatography (silica gel 60, 0.063-0.200 mm), these crude extracts were fractionated by gradient elution with an 10% (v/v) increase in proportion of acetone in DCM. Then, TLC (plastic backed plates coated with silica gel F_{254}) was used to monitor the 10 mL fractions (collected from the glass column and vanillin/H_2SO_4 solution (with heating) was used as visualizing agent. Under the appropriate solvent, fractions containing spots with similar R_f values were combined and undergo further purifi-

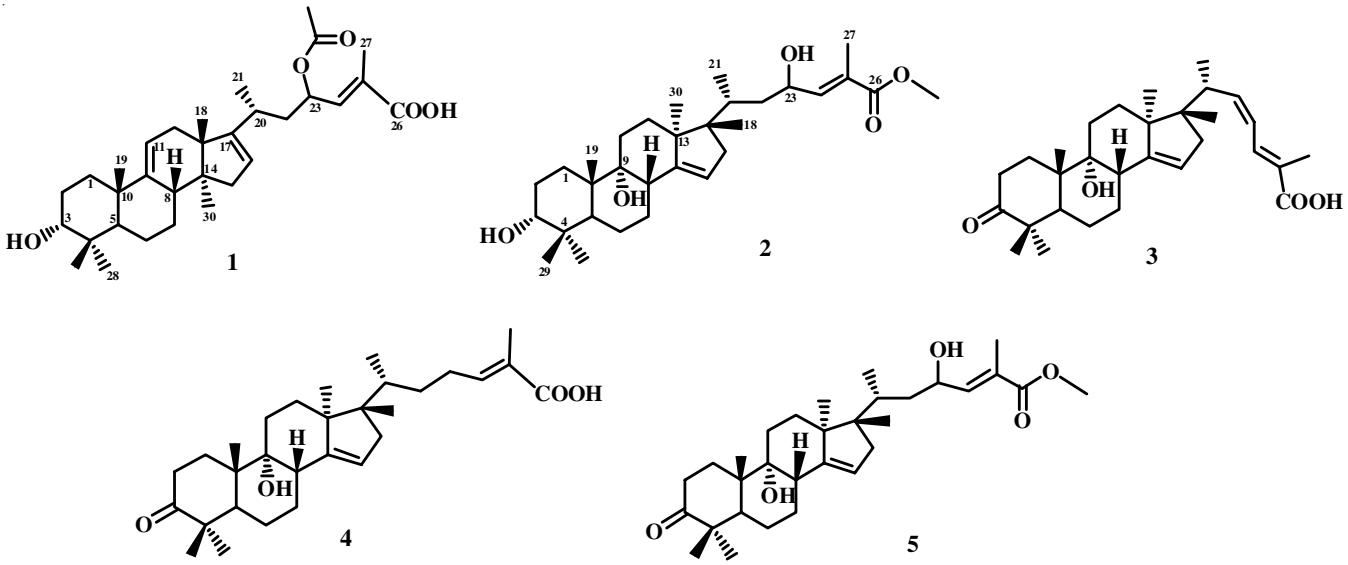

Fig. 1. Friedolanostanes identified from the extract of *G. benthamii*

cation process (rechromatographed). Afterwards, Pasteur pipettes were used for further chromatographic separations of the fractions and the pure isolates, which were verified *via* TLC, were collected, dried, and subjected to NMR analysis (Varian VNMRS spectrometer in $CDCl_3$ at 600 MHz for ^1H NMR and 150 MHz for ^{13}C NMR spectra).

Isolation of chemical constituents of the roots of *G. benthamii*: The DCM fraction from the chromatography of the crude root extract was rechromatographed using petroleum ether to afford squalene (0.5 mg). The 30% acetone fraction was rechromatographed using 5% EtOAc in petroleum ether to yield triacylglycerols (5.6 mg). The acetone fraction was rechromatographed using CH_3CN:Et_2O:CH_2Cl_2 (1:1:8, v/v) to yield compound **1** (1.3 mg) after washing with petroleum ether.

Isolation of chemical constituents of the fruit peel of *G. benthamii*: The DCM fraction from the chromatography of crude fruit peel extract was rechromatographed using petroleum ether to afford caryophyllene (106.7 mg) and squalene (1.4 mg). The 90% acetone in DCM fraction was rechromatographed using CH_3CN:Et_2O:CH_2Cl_2 (0.5:0.5:9, v/v), followed by CH_3CN:Et_2O:CH_2Cl_2 (1:1:8, v/v). The fractions eluted with CH_3CN:Et_2O:CH_2Cl_2 (0.5:0.5:9, v/v) afforded a mixture of compounds **1**, **3** and **4** (12.1 mg) after washing with petroleum ether. The fractions eluted with CH_3CN:Et_2O:DCM (1:1:8, v/v) yielded compound **2** (2.75 mg) after washing with petroleum ether.

Isolation of chemical constituents of the stem bark of *G. benthamii*: The DCM fraction from the chromatography of the crude stem bark extract was rechromatographed using petroleum ether to afford squalene (2.5 mg). The 30% acetone in DCM fraction was rechromatographed using 2.5% EtOAc in petroleum ether to yield friedelin (9.5 mg) after washing with petroleum ether. The 40% acetone in DCM fraction was rechromatographed in 5% EtOAc in petroleum ether, followed by 10% EtOAc in petroleum ether. The fractions eluted with 5% EtOAc yielded triacylglycerols (3.1 mg). The fractions eluted with 10% EtOAc in petroleum ether afforded a mixture of β-sitosterol and stigmasterol (0.8 mg). The 80% acetone in DCM fraction was rechromatographed using CH_3CN:Et_2O:DCM (0.5:0.5:9, v/v) to afford a mixture of compounds **3** and **5** (4.7 mg).

Isolation of chemical constituents of the leaves of *G. benthamii*: The DCM fraction from the chromatography of the crude leaf extract was rechromatographed using petroleum ether to afford caryophyllene (4.0 mg) and α-carotene (3.5 mg) after washing with petroleum ether. The 40% acetone in DCM fraction was rechromatographed using 15% EtOAc in petroleum ether to afford chlorophyll A (10.2 mg) after washing with petroleum ether. The 60% acetone in DCM fraction was rechromatographed using CH_3CN:Et_2O:CH_2Cl_2 (1:1:8, v/v) to yield compound **2** (5.6 mg) after washing with petroleum ether.

Isolation of chemical constituents of the flowers of *G. benthamii*: The 20% and 30% acetone in DCM fractions from the chromatography of the crude flowers extract were combined and rechromatographed using10% EtOAc in petroleum ether to yield a mixture of β-sitosterol and stigmasterol (4.4 mg) after washing with petroleum ether. The 50% and 60% acetone in DCM fractions were combined and rechromatographed using CH_3CN:Et_2O:CH_2Cl_2 (1:1:8, v/v) to yield compound **2** (6.2 mg).

Isolation of chemical constituents of flesh from the fruit of *G. benthamii*: The DCM and 10% acetone in DCM fractions were combined and rechromatographed using petroleum ether to afford squalene (2.1 mg). The 20% acetone in DCM was rechromatographed using 5% EtOAc in petroleum ether to yield tocotrienol (35.4 mg) after washing with petroleum ether. The 30% acetone in DCM fraction was rechromatographed using 5% EtOAc in petroleum ether to yield triacylglycerols (10.6 mg).

Isolation of chemical constituents of seeds of *G. benthamii*: The DCM and 10% acetone in DCM fractions were combined and rechromatographed using 5% EtOAc in petroleum ether to afford triacylglycerols (445.3 mg). The 20% acetone in DCM fraction was rechromatographed using 5% EtOAc in petroleum ether to yield a mixture of β-sitosterol and stigmasterol (29.3 mg).

Characterization data

(24*E*)-23-Acetoxy-3α-hydroxylanosta-9(11),16,24-trien-26-oic acid (1): Colourless amorphous solid; $[\alpha]_D^{25}$ = -224.8 (c = 0.1, methanol); UV ν_{max} = 248 nm; IR (neat, cm^{-1}): 3463 (OH), 1697 (C=O), 2969, 2931, 2873, 1454, 1334 (C-H), 1368, 1272, 1240 (OH); ^1H NMR (600 MHz) δ ppm: 6.63 (dq, *J* = 1.6, 9.0 Hz, H-24), 5.57 (ddd, *J* = 3.0, 6.0, 8.4 Hz, H-23), 5.29 (2H, br s, H-11, H-16), 3.42 (br s, H-3), 2.36 (m, H-8), 2.31 (m, H-12), 2.10 (br s, H-20), 2.08 (br s, H-15), 1.99 (2H, m, H-22, H-2), 1.85 (d, *J* = 1.2 Hz, H-15), 1.79 (m, H-1), 1.67 (3H, m, H-12, H-7, H-2), 1.57 (2H, m, H-22, H-6), 1.47 (2H, m, H-6, H-1), 1.38 (dd, *J* = 4.8, 12.5 Hz), 1.32 (dd, H = 2.4,9.6 Hz, H-5), 0.73 (s, Me-18), 1.06 (s, Me-19), 1.06 (d, *J* = 6.6 Hz, Me-21), 1.90 (d, *J* = 1.2 Hz, Me-27), 0.95 (s, Me-28), 0.88 (s, Me-29), 0.80 (s, Me-30), 2.03 (s, OAc); ^{13}C NMR (150 MHz) δ ppm: 30.55 (C-1), 25.66 (C-2), 76.25 (C-3), 37.90 (C-4), 46.69 (C-5), 21.06 (C-6), 27.94 (C-7), 40.05 (C-8), 149.62 (C-9), 39.61 (C-10), 114.07 (C-11), 31.20 (C-12), 46.72 (C-13), 50.94 (C-14), 40.38 (C-15), 120.86 (C-16), 155.27 (C-17), 19.68 (C-18), 21.98 (C-19), 28.10 (C-20), 20.85 (C-21), 40.88 (C-22), 69.16 (C-23), 141.19 (C-24), 129.37 (C-25), 170.33 (C-26), 12.94 (C-27), 28.36 (C-28), 22.55 (C-29), 19.95 (C-30), 21.14, 170.33 (OAc).

Methyl(24*E*)-3α,9α,23-trihydroxy-17,14-friedolanosta-14,24-dien-26-oate (2): ^1H NMR (600 MHz) δ ppm: 6.68 (1H, dq, *J* = 1.6, 7.8 Hz, H-24), 5.31 (br s, H-15), 4.54 (ddd, *J* = 1.6, 8.4, 10.8 Hz, H-23), 3.36 (br s, H-3), 0.74 (s, Me-18), 0.90 (s, Me-19), 0.90 (d, *J* = 6.6 Hz, Me-21), 1.85 (d, *J* = 1.2 Hz, Me-27), 0.83 (s, Me-28), 0.94 (s, Me-29), 1.20 (s, Me-30), 3.73 (s, OMe); ^{13}C NMR (150 MHz) δ ppm: 23.60 (C-1), 25.11 (C-2), 76.08 (C-3), 37.52 (C-4), 39.03 (C-5), 20.78 (C-6), 25.69 (C-7), 39.14 (C-8), 75.37 (C-9), 42.17 (C-10), 29.58 (C-11), 29.01 (C-12), 49.08 (C-13), 153.53 (C-14), 120.43 (C-15), 44.72 (C-16), 53.99 (C-17), 15.34 (C-18), 16.39 (C-19), 33.96 (C-20), 15.08 (C-21), 39.11 (C-22), 66.78 (C-23), 144.38 (C-24), 127.12 (C-25), 168.46 (C-26), 12.72 (C-27), 28.47 (C-28), 22.01 (C-29), 19.41 (C-30), 51.94 (OMe).

(22*Z*,24*E*)-9α-Hydroxy-3-oxo-17,14-friedolanosta-14, 22,24-trien-26-oic acid (3): ^1H NMR (600 MHz) δ ppm: 5.29

(br s, H-15), 0.72 (s, Me-18), 0.87 (s, Me-19), 0.92 (d, *J* = 7.2 Hz, Me-21), 5.96 (t, *J* = 10.8 Hz, H-22), 6.20 (t, *J* = 11.4 Hz, H-23), 7.64 (d, *J* = 12 Hz, H-24), 1.92 (br s, Me-27), 1.06 (s, Me-28), 1.02 (s, Me-29), 1.06 (s, Me-30); ^{13}C NMR (150 MHz) δ ppm: 29.78 (C-1), 34.36 (C-2), 217.17 (C-3), 47.46 (C-4), 45.92 (C-5), 21.95 (C-6), 29.92 (C-7), 39.21 (C-8), 75.31 (C-9), 41.94 (C-10), 24.92 (C-11), 27.33 (C-12), 49.22 (C-13), 152.75 (C-14), 120.89 (C-15), 44.17 (C-16), 53.83 (C-17), 15.62 (C-18), 16.63 (C-19), 36.94 (C-20), 17.69 (C-21), 143.95 (C-22), 121.95 (C-23), 134.97 (C-24), 126.34 (C-25), 173.37 (C-26), 12.12 (C-27), 26.24 (C-28), 21.29 (C-29), 19.28 (C-30).

(24*E*)-9α-Hydroxy-3-oxo-17,14-friedolanosta-14,24-dien-26-oic acid (4): ^{1}H NMR (600 MHz) δ ppm: 5.36 (d, *J* = 7.8 Hz, H-15), 0.72 (s, Me-18), 1.04 (s, Me-19), 0.84 (d, *J* = 6.6 Hz, Me-21), 6.90 (t, *J* = 7.2 Hz, H-24), 1.92 (br s, Me-27), 1.06 (s, Me-28), 1.02 (s, Me-29), 1.06 (s, Me-30); ^{13}C NMR (150 MHz) δ ppm: 29.69 (C-1), 34.32 (C-2), 217.05 (C-3), 47.45 (C-4), 45.99 (C-5), 21.95 (C-6), 29.92 (C-7), 39.21 (C-8), 75.18 (C-9), 41.48 (C-10), 24.92 (C-11), 27.42 (C-12), 49.07 (C-13), 152.48 (C-14), 121.44 (C-15), 44.17 (C-16), 54.57 (C-17), 15.37 (C-18), 16.56 (C-19), 22.12 (C-20), 15.12 (C-21), 28.86 (C-22), 30.37 (C-23), 145.38 (C-24), 126.80 (C-25), 172.23 (C-26), 11.97 (C-27), 26.18 (C-28), 21.29 (C-29), 19.28 (C-30).

Methyl (24*E*)-9,23-dihydroxy-3-oxo-17,14-friedolanosta-14,24-dien-26-oate (5): ^{1}H NMR (600 MHz) δ ppm: 5.36 (br m, H-15), 0.76 (s, Me-18), 1.05 (s, Me-19), 0.80 (d, *J* = 6.6 Hz, Me-21), 4.54 (ddd, *J* = 1.6, 8.4, 10.8 Hz, H-23), 6.69 (dq, *J* = 1.8, 8.4 Hz, H-24), 1.85 (d, *J* = 1.2 Hz, Me-27), 1.07 (s, Me-28), 1.02 (s, Me-29), 1.23 (s, Me-30), 3.74 (s, OCH_3); ^{13}C NMR (150 MHz) δ ppm: 29.65 (C-1), 34.32 (C-2), 217.05 (C-3), 47.46 (C-4), 45.97 (C-5), 21.96 (C-6), 29.79 (C-7), 39.21 (C-8), 75.18 (C-9), 41.85 (C-10), 24.93 (C-11), 27.42 (C-12), 49.08 (C-13), 142.47 (C-14), 121.45 (C-15), 44.74 (C-16), 54.15 (C-17), 15.38 (C-18), 16.57 (C-19), 31.97(C-20), 17.69 (C-21), 39.21 (C-22), 66.75 (C-23), 144.26 (C-24), 126.16 (C-25), 171.66 (C-26), 12.74 (C-27), 26.19 (C-28), 21.30 (C-29), 19.95 (C-30), 51.96 (OCH_3).

Ligands and protein preparation: The sdf file of dexamethasone (control) was obtained from https://pubchem.ncbi.nlm.nih.gov/ while Compounds **1-5** were drawn in ChemSketch Version 12.01 [15]. These structures were further trimmed by the "3D optimization" feature in the 3D viewer of Chemsketch and saved in mol format. All ligand files were converted to pdbqt format by using Open Babel software [7].

On the other hand, the pdb file of NF-κB p50 homodimer (PDB: 1SVC) was downloaded from PDB database on https://www.rcsb.org/. The native ligand (DNA) bound to p50 including water molecules were removed through Biovia Discovery Studio 2021 Client [16]. The grid position was aligned to the position of the native ligand present on the binding site prior to removal of the bound ligand. Then, the processed p50 was further optimized on AutoDock Tools to add polar hydrogen and Kollman charges. Lastly, the fully optimized p50 was saved in pdbqt format.

Prior to performing *in silico* analysis, the pdb file of the processed p50 protein was uploaded to Ramachandran Plot server [17] and MolProbity [18] to validate the structure of the prepared protein. Afterwards, the results for ERRAT [18] and Verify 3D [18] programs were generated through MolProbity and a Ramachandran plot [17] of the protein model was obtained.

Molecular docking study: For this study, the operating system used was Windows 10 with AMD Ryzen 7 3700U, Radeon Vega Mobile Gfx 2.30 GHz and RAM of 8.00 GB. Before performing the docking analysis in Autodock Vina, the grid parameters were set as 20, 20, 20 x, y, z size and 27.702003, 30.851276 and 27.702665 x, y, z center-coordinates. Exhaustiveness was set at default 8. Docking results were visualized using Discovery Studio Visualizer [16].

Molecular dynamics analysis: From the results of molecular docking analysis, the promising compounds complexed with p50 were subjected to molecular dynamics study in CABS Flex 2.0 server [19]. Based on the coarse-grained simulation of the protein-ligand binding, the stability of the protein during the interaction would be reflected in the RMSF data obtained. Moreover, the protein-ligand interaction model (10 ns) revealed the highly interacting amino acids on the binding site of the p50 homodimer.

Pharmacophore modeling: For this purpose, PharmaGist [13] was used by uploading the mol2 files of the promising compounds to the server. The output data file would show the pharmacophore descriptors present in the compounds. The pharmacophore descriptors for each compound where annotated and visualized by Discovery Studio Visualizer.

Investigating pharmacokinetic properties: Using the software Open Babel [19], the SMILES [20,21] connotation of the compounds was obtained by converting from mol files. The SMILES connotations were submitted to ADMETlab [13] (https://admetmesh.scbdd.com/) to predict the drug-likeness and ADMET properties of the friedolanostanes.

RESULTS AND DISCUSSION

Silica gel chromatography of the DCM extract of *Garcinia benthamii* yielded a new triterpene (24*E*)-23-acetoxy-3α-hydroxylanosta-9(11),16,24-trien-26-oic acid (**1**), squalene and triacylglycerols from the roots; methyl (24*E*)-3α,9α,23-trihydroxy-17,14-friedolanosta-14,24-dien-26-oate (**2**), caryophyllene, squalene, a mixture of compound **1**, (22*Z*,24*E*)-9α-hydroxy-3-oxo-17,14-friedolanosta-14,22,24-trien-26-oic acid (**3**) and another new triterpene (24*E*)-9α-hydroxy-3-oxo-17,14-friedolanosta-14,24-dien-26-oic acid (**4**) from the fruit peel; a mixture of compound **3** and a new triterpene methyl (24*E*)-9α,23-dihydroxy-3-oxo-17,14-friedolanosta-14,24-dien-26-oate (**5**), friedelin, squalene, triacylglycerols and a mixture of β-sitosterol and stigmasterol from the stem bark; compound **2**, caryophyllene, α-carotene and chlorophyll a from the leaves; Compound **2** and a mixture of β-sitosterol and stigmasterol from the flowers; δ-tocotrienol, squalene and triacylglycerols from the flesh of fruit; and triacylglycerols and a mixture of stigmasterol and β-sitosterol from the seeds of *G. benthamii*. Compound **2** was in concurrence with the results found in a published work [22] characterizing methyl (24*E*)-3α,9α,23-trihydroxy-17,14-friedolanosta-14,24-dien-26-oate. The resulting NMR data for (22*Z*,24*E*)-9α-hydroxy-3-oxo-17,14-friedo-

lanosta-14,22,24-trien-26-oic acid (**3**) [23]; squalene [24]; triacylglycerols [25]; caryophyllene [26]; friedelin [27]; β-sitosterol [28]; stigmasterol [28]; α-carotene [28]; chlorophyll a [29] and δ-tocotrienol [30] were also compared with existing published works. The structures of friedolanostanes (**2-5**) were characterized through in depth 1D and 2D NMR techniques. Thus, distinct chemical shift from the generated NMR spectra were summarized and presented below starting from the most deshielded to least deshielded.

NMR analysis: The ^{1}H NMR spectrum of compound **1** gave resonances for two overlapping olefinic protons at δ 5.29 and another olefinic proton at δ 6.63 ppm; a methine proton of an alcohol at δ 3.42 and an allylic methine proton of an acetate at δ 5.57; an acetate methyl at δ 2.03, an allylic methyl at δ 1.90, five methyl singlets at δ 0.73, 0.80, 0.88, 0.95 and 1.06 and a methyl doublet at δ 1.06.

The ^{13}C NMR spectrum of **1** indicated resonances for two oxymethine carbons at δ 76.25 and 69.16 ppm; six olefinic carbons at δ 114.07, 120.86, 129.37, 141.19, 149.62 and 155.27 ppm; overlapping resonances for carbonyl carbons of a carboxylic acid and an acetate at δ 170.33 ppm; eight methyl carbons at δ 12.94, 19.68, 19.95, 20. 85, 21.14, 22.55, 28.36 and 28.56 ppm; seven methylene carbons; three additional methine carbons; and four additional quaternary carbons. These resonances indicated a triterpene with an alcohol, an acetate, a carboxylic acid and three double bonds. The correlation spectroscopy (COSY) analysis (Fig. 2a) indicated 5 isolated spin systems as follows: H_2-1/H_2-2/H-3; H-5/H_2-6/H_2-7/H-8; H-11/H_2-12; H_2-15/H-16; H_3-21/H-20/H_2-22/H-23/H-24/H_3-27. Yet, many of the methylene protons present in the molecule do overlap in a certain region that causes peaks to appear as a multiplet. Thus, these overlapping regions do also cause the difficulty to establish the chemical shifts of the said protons. To correlate the attached protons to their corresponding carbons, heteronuclear single quantum coherence (HSQC) 2D NMR data of compound **1** was used. Assigned chemical shift for all protons is listed in the second column of Table-1. As observed, the allylic proton (H-15) and olefinic proton (H-16) do exhibit a multiplicity of broad singlet because of the small coupling constant for allylic coupling.

Based on the long-range correlation observed in heteronuclear multiple bond coherence (HMBC) 2D NMR data, the isolated spin systems were connected. These correlations were highlighted in Fig. 2a and listed as hydroxyl carbon (C-3) was correlated to the oxymethine proton (H-3) and the methyl carbons (C-28 and C-29); the olefinic protons (δ 5.29) was attached to C-11 (correlated to C-8, C-9, C-10 and C-12) and C-16 (correlated to C-13, C-14, C-15, C-17 and C-20) due to their correlation to the nearby carbons; olefinic proton (δ 6.63) was attached to

TABLE-1
RELATIVE COSY AND HMBC SIGNALS OF COMPOUND **1**

Atom	^{1}H Shifts (δ)	^{1}H Shifts correlation (δ)	Correlated ^{13}C shifts (δ)	
			^{2}J	^{3}J
24	6.63	5.57, 1.90	170.33	12.94, 170.33
23	5.57	6.63, 1.99, 1.57	141.19, 170.33	28.10, 129.37
11	5.29	2.31, 1.67	31.20, 149.62	31.20, 39.61, 40.05
16	5.29	2.08, 1.85	40.88	46.72, 50.94
3	3.42	1.99, 1.67	46.49	30.55
8	2.36	1.67, 1.38	50.94, 149.62	19.95, 114.07
12	2.31 1.67	5.29, 0.73,1.67 5.29, 0.73, 2.31	114.07	149.62, 19.95
20	2.10	5.57, 2.08, 1.85, 1.99, 1.57, 1.06	155.27, 20.85	69.16
15	2.08 1.85	5.29, 2.10, 1.06 (d), 1.85 5.29, 2.10, 1.06 (d), 2.08	120.86	40.05, 46.72, 40.05, 19.95, 155.27
CH_3COO-	2.03	5.57	170.33	–
2b	1.99	3.42, 1.67, 1.47, 1.79	–	–
22b	1.99	1.57, 2.10, 5.57	28.10, 69.16	20.85, 141.19,
27	1.90	6.63	129.37	141.19, 170.33
15	1.85	2.08	50.94, 120.86	46.72, 155.27, 19.95
1	1.79	1.06, 1.47, 1.67, 1.99	25.66	–
6b	1.57	1.67, 1.47, 1.32	27.94	–
22a	1.57	1.90, 2.10, 5.57	28.10, 69.16	20.85, 141.19,
2a	1.67	1.99, 1.47, 1.79	76.25, 30.55	76.25, 30.55
7b	1.67	2.36, 1.57, 1.38, 1.47	–	–
12	1.67	3.42, 2.31, 5.29	46.72, 114.07	19.68, 50.94,149.62
7a	1.38	2.36, 1.67, 1.57, 1.47	–	–
1	1.47	1.99, 1.67, 1.79	25.66	–
6a	1.47	1.57, 1.38, 1.67, 1.32	–	–
5	1.32	1.57, 1.47	21.06, 37.90, 39.61	21.98, 27.94
19	1.06	1.79	39.61	21.06, 30.55, 46.69, 149.62
21	1.06 (d)	2.10	28.10	155.27, 40.38
30	0.80	2.08	50.94	40.88, 27.94
29	0.88	–	37.90	22.55, 46.69, 76.25
28	0.95	–	37.90	22.55, 46.69, 76.25
18	0.73	2.31	46.72	31.20, 50.94, 155.27

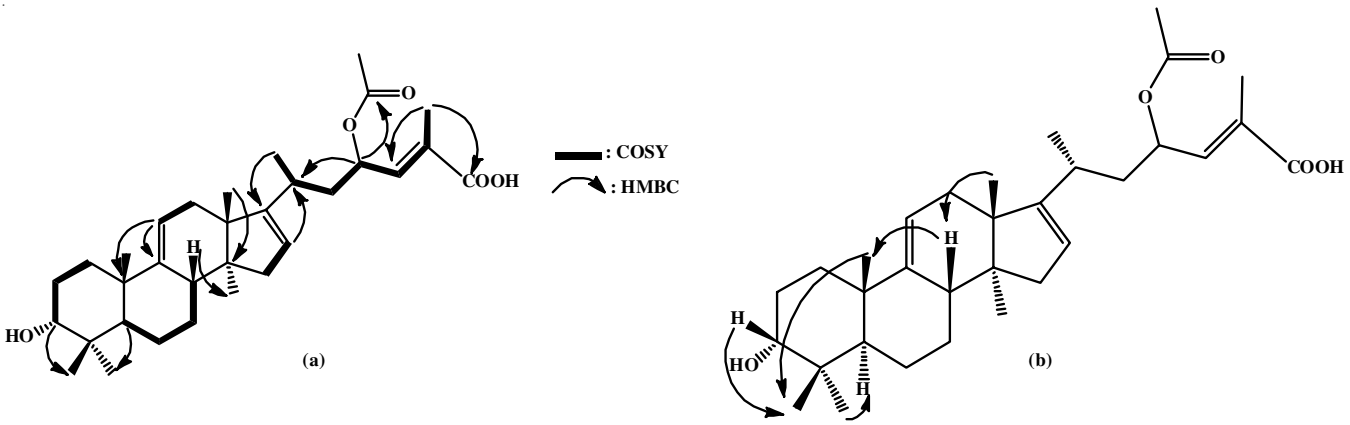

Fig. 2. (a) ^{1}H-^{1}H COSY and ^{1}H-^{13}C long-range correlations (b) NOESY correlations for **1**

C-24 due to its correlation to C-22, C-23, C-25, C-26 and C-27. The allylic methyl was assigned to C-27 since long-range correlations were observed between this methyl and the olefinic carbons (C-24 and C-25) and the carboxylic acid (C-26). The acetate was attached to C-23 based on long-range correlations between the oxymethine proton (H-23) and the carboxylate. The relative configuration of compound **1** (Fig. 2b) was deduced from Nuclear Overhauser effect spectroscopy (NOESY) analysis. The methyl singlet (H_3-29) was close in space to H-3 and another methyl singlet (H_3-19), which was in turn close to the methine proton (H-8), which was finally close to the methyl singlet (H_3-18). On the opposite face of compound **1**, the methyl singlet (H_3-28) was close in space to the methine proton (H-5). All NOESY correlations observed were consistent with the relative configuration of compound **1**.

The structure of compound **1** was confirmed by high resolution electron spray ionization mass spectrometry (HRESI-MS) analysis which revealed a pseudo molecular ion of *m/z* 513.3582 $[M+H]^+$, corresponding to a molecular formula of $C_{32}H_{49}O_5$. Literature search revealed that compound **1** is a new compound and th trivial name ragasolide is proposed for compound **1**.

Compound **4** was obtained as a mixture with compounds **1** and **3** from the fruit peel. Compound **4** showed relatively similar resonances with **3**. The difference lies in the non-appearance of a double bond at C-22 in compound **4**. On the other hand, compound **5** was obtained as a mixture with compound **3** from the stem bark. The difference lies in the conversion of hydroxyl at C-3 in compound **2** to carbonyl in compound **5**. Furthermore, a range of chemical shifts was assigned to the methylene protons (Table-2), due to the sample complexity and proton environment.

***In silico* investigation of potential anti-inflammatory property of friedolanostanes:** The prepared protein model was validated through different algorithms to ensure the structural reliability of the protein's 3D structure. The generated Ramachandran plot [17] (Fig. 3a) from the web server shows that 94.36% of the residues were found in the favourable region. The protein model had a reasonable main-chain and side-chain conformation [31]. Additionally, the prepared protein was further subjected to analysis through MolProbity [18]. Based on the Verify3D result (Fig. 3b), the processed protein model afforded a highly compatible 3D structure attested by 99.04% of the residues having obtained an average 3D/1D profile score of ≥ 0.2). Moreover, the protein model was well-folded since the score rarely dropped below 0.1 (Fig. 3b). This observation did conform with the mentioned property of a well-refined protein structure from an earlier study [32]. An extension to the Verify3D [18] analysis within Molprobity named ERRAT [18] was performed on the p50 protein model to verify its structure and non-bonded atom-atom interaction (Fig. 3c). With an overall quality factor greater than 50%, the prepared p50 protein model (80.54%) was considered to pass the evaluation [33]. Considering all the three factors, the structure of the prep-

TABLE-2
CHEMICAL SHIFT OF THE METHYLENE PROTONS FROM COMPOUNDS **2**, **3**, **4** AND **5**

Atom	^{1}H Shifts (δ)			
	2	**3**	**4**	**5**
1	1.05-1.16, 1.88-1.98	1.62-1.66	1.60-1.65	1.62-1.66
2	1.34-1.65, 1.88-198	2.30-2.44, 2.50-2.57	2.32-2.43, 2.50-2.56	2.30-2.44, 2.50-2.57
5	1.91-2.00	2.06-2.08	2.06-2.10	2.06-2.08
6	1.34-1.40	1.50-1.54, 1.62-1.66	1.46-1.50, 1.60-1.65	1.50-1.64, 1.62-1.66
7	1.34-1.65, 1.88-1.98	1.62-1.66, 2.06-2.08	1.60-1.65, 2.06-2.10	1.62-1.66, 2.06-2.08
8	2.31-2.35	2.30-2.44	2.32-2.43	2.30-2.44
11	1.34-1.65, 1.76-1.81	2.06-2.08	2.06-2.10	2.06-2.08
12	1.51-1.54	1.30-1.33, 1.62-1.66	1.30-1.33, 1.60-1.65	1.30-1.33, 1.62-1.66
16	1.76-1.82, 2.31-2.35	1.82-1.85	1.82-1.85	1.76-1.82, 2.30-2.33
20	2.23-2.30	3.18-3.25	1.93-2.02	2.24-2.30
22	1.03-1.13, 1.63-1.73	(Alkenyl hydrogen)	2.04-2.10	1.06-1.13, 1.63-1.73
23	(Oxymethine)	(Alkenyl hydrogen)	2.23-2.28	(Oxymethine)

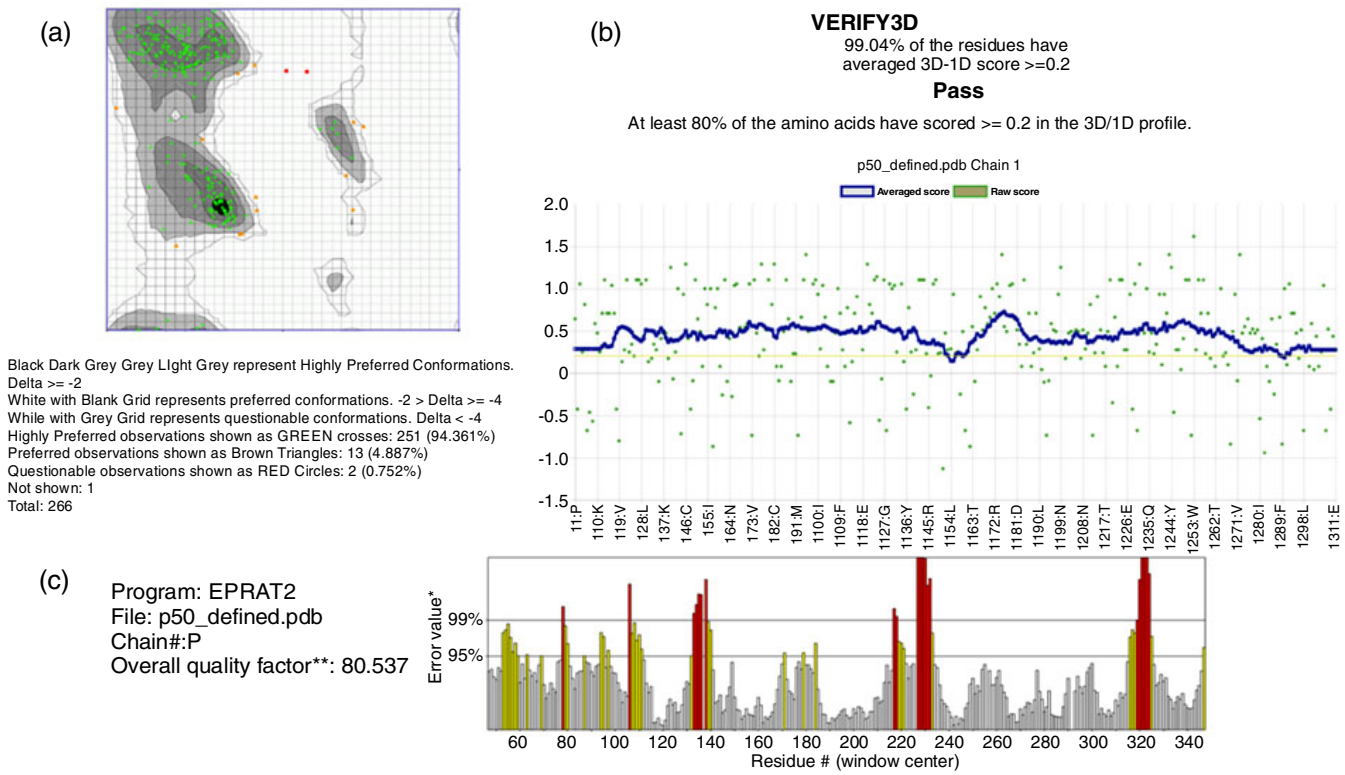

Fig. 3. Structure validation of the p50 protein: (a) Verify 3D; (b) ERRAT; and (c) Ramachandran plot

ared p50 protein model was substantiated for the subsequent molecular docking analysis.

All the 5 friedolanostanes identified were analyzed for their binding affinity with the NF-kB p50 homodimer. Compounds **4** and **5** (Table-3) had the highest binding affinity (-4.1 kcal/mol) to the target protein as compared to the control dexamethasone (-3.7 kcal/mol). This was followed by compound **2** with -3.8 kcal/mol while compound **1** afforded -3.6 kcal/mol. The binding energy of dexamethasone was used as a cut-off reference value for further *in silico* investigation of compounds **2-5** for their interactions within the p50 binding pocket. The interaction between p50 and compound **5** is presented in Fig. 4.

Among the 310 amino acid residues, a total of 9 (Arg 57, Tyr 60, Glu 63, Lys 244, Pro 246, Lys 275, Arg 308, Gln 309 and Phe 310) were observed to interact with compounds **2-5** (Table-4). Based on the Ramachandran plot, most of the interacting amino acid residues were found in a-helix area (Glu 63, Lys 244, Pro 246, Phe 310), with three (Arg 57, Tyr 60, Lys 275) in the b-sheet and two (Arg 308 and Gln 309) in the left-handed helix (Fig. 4c). These amino acids interacted with the ligands through conventional hydrogen bonding and van der Waals forces (Fig. 4b). The amino acids present in the hydrophobicity pocket (Tyr 60, Glu 63, Arg 308, Gln 309) were observed to interact by van der Waals attractions (Fig. 4d). Two of the hydrophilic amino acids (Arg 57 and Lys 244) were observed to interact with the hydrogen-acceptor or donating sites of the ligands (Fig. 4e). The specific pharmacophore descriptors of the ligands **2-5** and the positive control dexamethasone were marked and presented in Fig. 5. These descriptors provide information of which part of the ligand will most likely form interactions with the amino acid residues in the binding pocket of the NF-kB p50 protein.

Molecular dynamics simulation: A 10 ns molecular dynamics simulation (MDS) was generated per protein-ligand complex. These were compared with the MDS model obtained from the p50 apo-protein (unbound). The RMSF of the p50-

TABLE-3
BINDING ENERGY OF THE COMPOUNDS TO p50 HOMODIMER AND THEIR DRUG-LIKENESS BASED ON LIPINSKI'S RULE OF FIVE WITH REFERENCE VALUES INDICATED: MW, MOLECULAR WEIGHT; Log P, LIPOPHILICITY; HBD, HYDROGEN BOND DONOR; HBA, HYDROGEN BOND ACCEPTOR; TPSA, TOPOGRAPHICAL SURFACE AREA

Compound	Binding energy (kcal/mol)	m.f.	Lipinski's rule of five				
			MW (Da) ≤ 500	log P ≤ 5	HBD ≤ 5	HBA ≤ 10	TPSA (Å^2) ≤ 140
Dexamethasone (Control)	-3.7	$C_{22}H_{29}O_5F$	394.51	1.9	3	5	94.8
1	-3.6	$C_{32}H_{48}O_5$	512.81	6.8	2	4	83.8
2	-3.8	$C_{31}H_{50}O_5$	502.81	5.6	3	5	87.0
3	-3.7	$C_{30}H_{44}O_4$	468.74	6.5	2	3	74.6
4	-4.1	$C_{30}H_{46}O_4$	470.76	6.7	2	3	74.6
5	-4.1	$C_{31}H_{48}O_5$	500.79	5.8	2	5	83.8

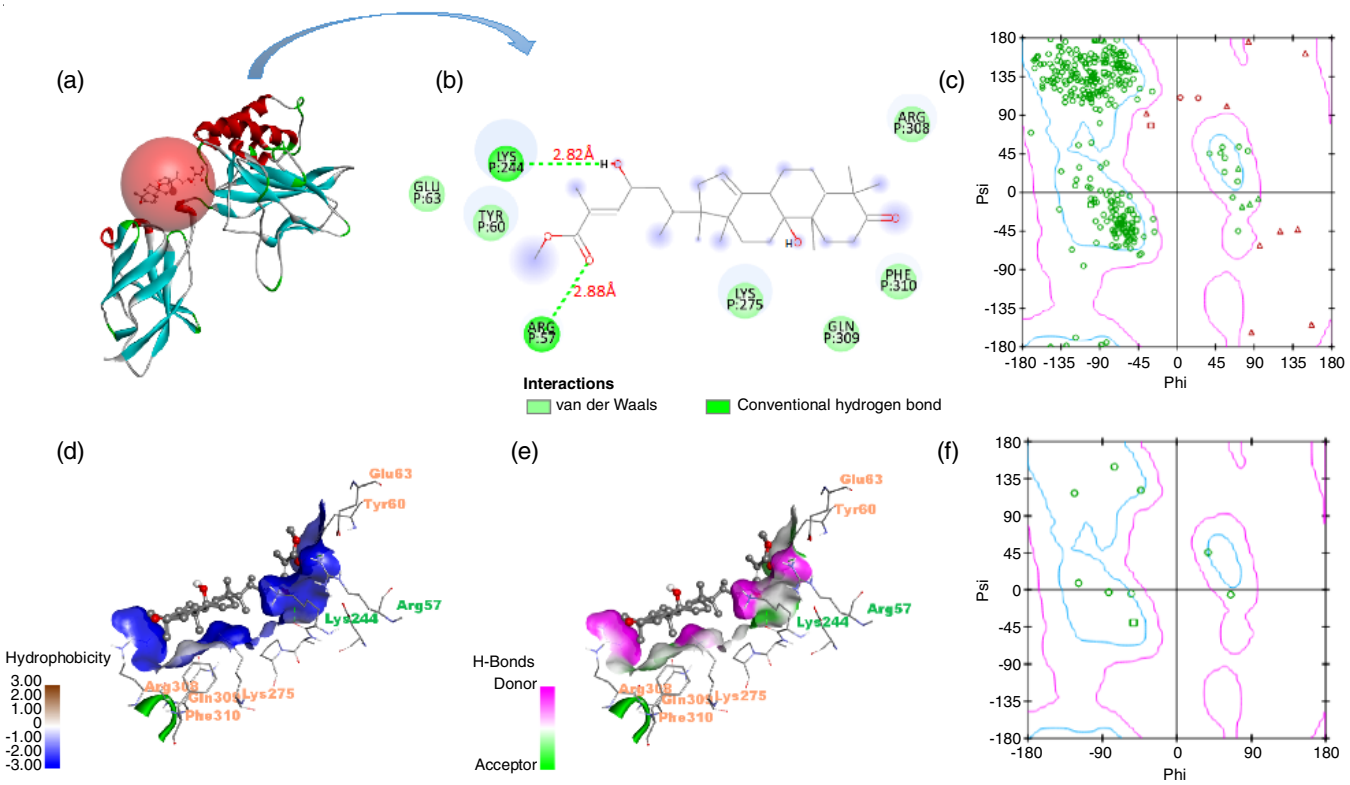

Fig. 4. Interaction of compound **5** in the NF-kB p50 binding site: (a) the defined binding sphere with the ligand; (b) two-dimensional display of the interaction; (c) Ramachandran plot of p50; (d) hydrophobic property of binding pocket; (e) H-bond property of binding pocket; and (f) Ramachandran plot of ligand-interacting amino acid residues

TABLE-4
AMINO ACID RESIDUES OF p50 HOMODIMER WITH THE TOP BINDING FRIEDOLANOSTANES IN *G. benthamii Pierre*

Compound	Interacted residues	Residues involved in hydrogen bonding	Residues involved in van der Waals
2	Arg 57, Tyr 60, Glu 63, Lys 244, Lys 275, Arg 308, Gln 309, Phe 310	Arg 57 (3.02 Å)	Tyr 60, Glu 63, Lys 244, Lys 275, Arg 308, Gln 309, Phe 310
3	Arg 57, Tyr 60, Glu 63, Lys 244, Pro 246, Lys 275, Arg 308, Gln 309, Phe 310	Arg 57 (3.02 Å)	Tyr 60, Glu 63, Lys 244, Pro 246, Lys 275, Arg 308, Gln 309, Phe 310
4	Arg 57, Tyr 60, Glu 63, Lys 244, Lys 275, Arg 308, Gln 309, Phe 310	Arg 57 (2.85Å), Lys 244 (3.08 Å)	Tyr 60, Glu 63, Lys 275, Arg 308, Gln 309, Phe 310
5	Arg 57, Tyr 60, Glu 63, Lys 244, Lys 275, Arg 308, Gln 309, Phe 310	Arg 57 (2.88 Å), Lys 244 (2.82 Å)	Tyr 60, Glu 63, Lys 275, Arg 308, Gln 309, Phe 310

compound **5** complex and the p50 apo-protein during the 10 ns period of simulation are presented in Fig. 6a. While fluctuations were observed in Asn 78 (turn), Lys 147 (helix), Lys 148 (helix), Gly 165 (turn), Ala 245 (coil), Pro 246 (helix), Asn 247 (helix) and 264 (turn) amino acid residues in p50-compound **5** complex, the average RMSF descriptors were calculated to be 0.89 ± 0.7 Å compared with 0.88 ± 0.7 Å for the p50 apo-protein, which suggested structural integrity of the protein. The average RMSF descriptors of other complexes are listed in Table-5. The structural comparisons showed that upon ligand binding no significant conformational changes took place in the p50 protein structure. The overall stability of the complex was maintained without any remarkable deviation compared to the p50 apo-protein (Fig. 6b).

Drug-likeness and pharmacokinetic properties of the friedolanostanes: The Lipinski's rule of five recommends that for a compound to have "druggability", there should be no more than one violation of the following: molecular weight (MW) of ≤ 500 Da, log P value ≤ 5, number of H-bond donor (HBD) ≤ 5. and H-bond acceptor (HBA) ≤ 10 and topological surface area of (TPSA) ≤ 140 $Å^2$ [30]. Compounds **3** and **4** passed the druggability criteria based on only a single violation which is high log P whereas compounds **1**, **2** and **5** afforded two violations involving high log P and MW values (Table-3).

TABLE-5
AVERAGE RMSF DESCRIPTORS OF THE p50 apo-PROTEIN AND p50 PROTEIN-LIGAND COMPLEXES

Complex	Average RMSF descriptors	P value
p50 apo-protein	0.89 ± 0.7 Å	(Reference)
p50-2	0.90 ± 0.8 Å	0.1393
p50-3	0.93 ± 0.9 Å	0.8239
p50-4	0.94 ± 1.0 Å	0.6481
p50-5	0.89 ± 0.7 Å	0.0576

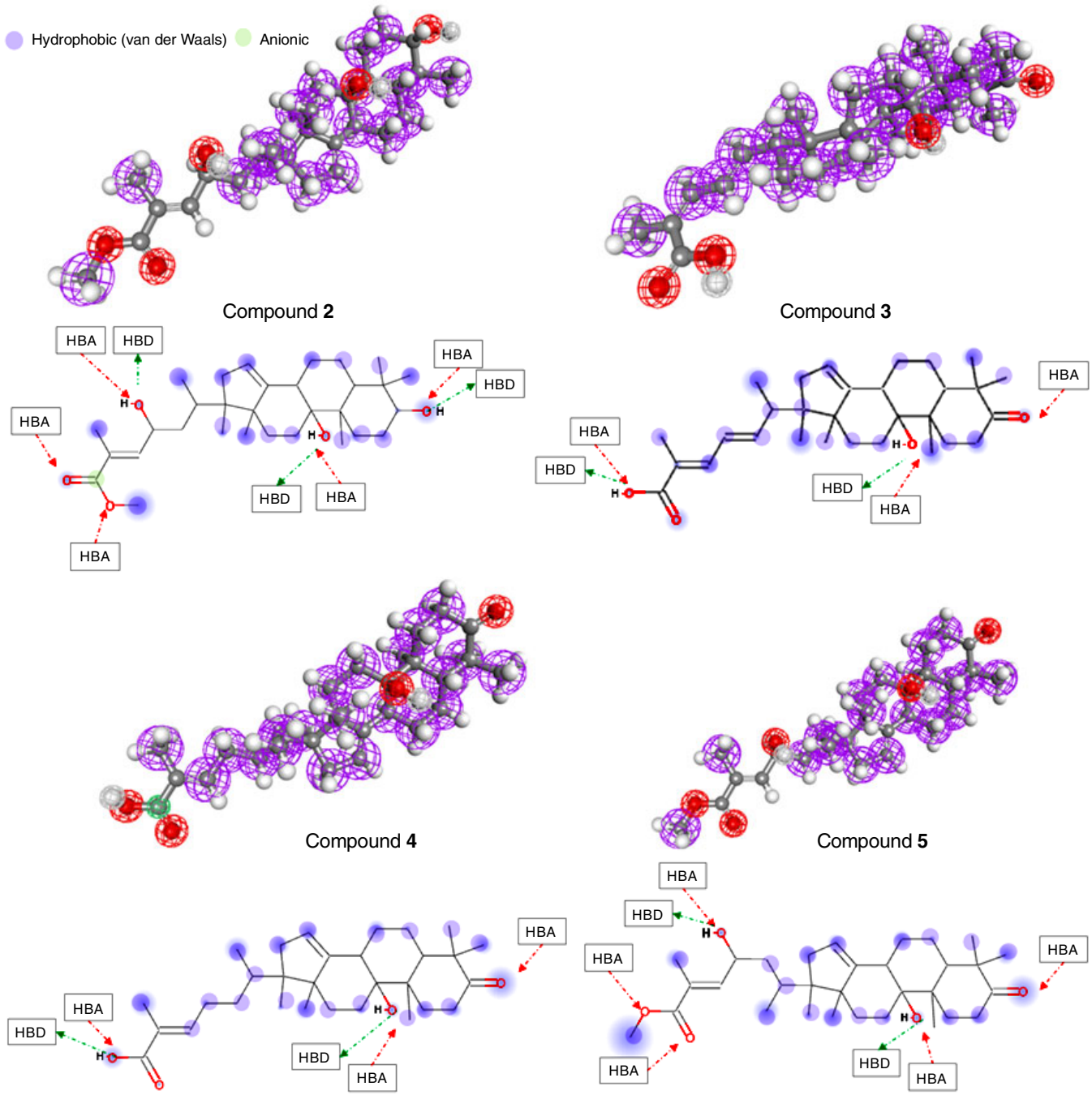

Fig. 5. Pharmacophore descriptors of the friedolanostanes (compounds **2**-**5**)

While the Lipinski's rule is generally not definitive [30], there are some compounds with high log P values that are currently marketed drugs [34]. This suggests that compounds **1**-**5** should not be excluded for further testing. Furthermore, Doak *et al.* [34] proposed a new considerable limit for the drug-likeness properties of compounds based on their analysis of approved oral drugs and other candidates. Their study stated that the log P value could be as low as -2 but not more than 10. Considering these parameters, compounds **1**-**5** should still be considered for further drug discovery studies.

The deduced ADMET properties of the compounds and dexamethasone were summarized and presented as a heatmap (Fig. 7). As shown in the predicted metabolism profile, there was a moderate probability that these compounds could be metabolized through the enzymatic action of cytochrome-P450. Cytochrome-P450 is an enzyme complex necessitous for the metabolism and detoxification of xenobiotics and other foreign substances. Drug molecules that can repress this enzyme complex can persist longer and thus have higher likelihood of reaching the intended target [35]. Moreover, unlike dexamethasone, these compounds are Pgp inhibitors and plasma protein binders, which may enhance their bioavailability and distribution [35]. The physico-chemical properties of these compounds also demonstrated limited water solubility and permeability, which

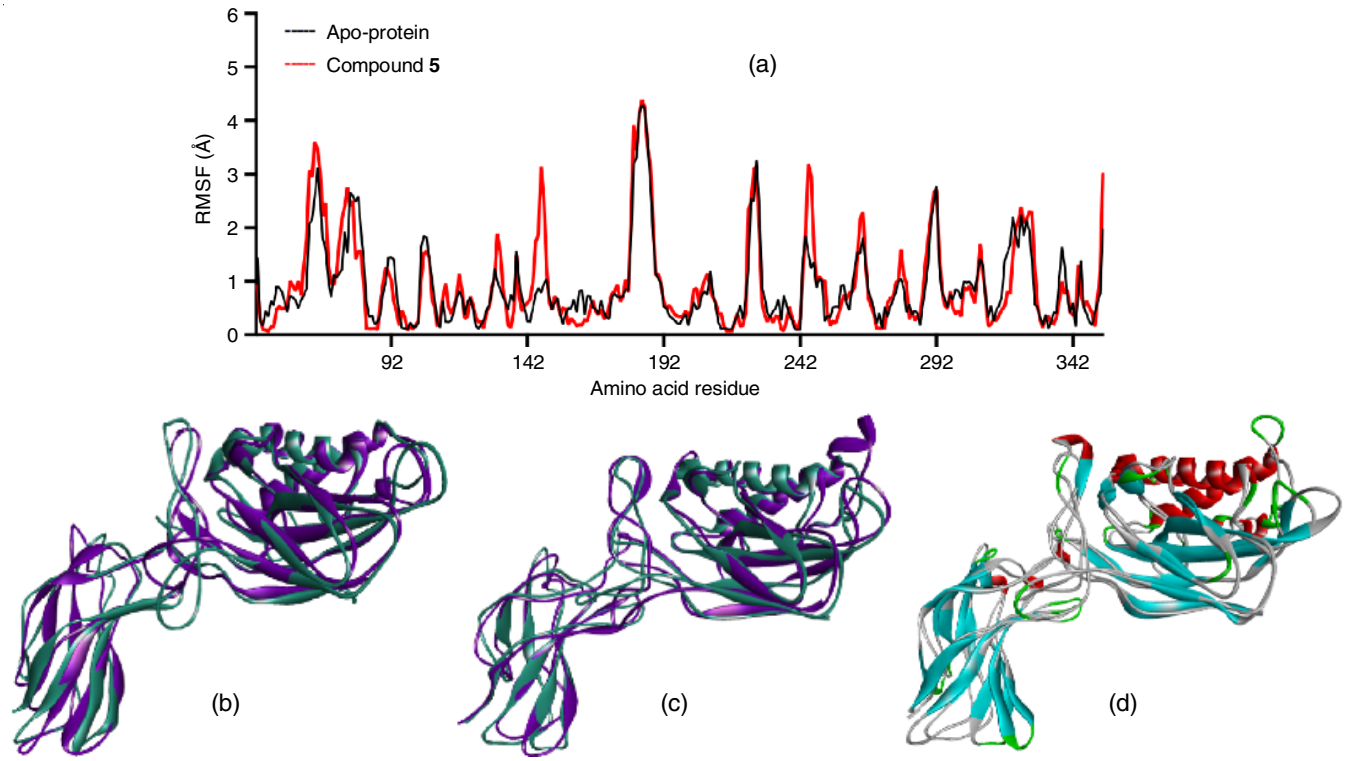

Fig. 6. (a) RMSF values of amino acid residues of p50 apo-protein (unbound) and p50-compound **5** complex. Corresponding superimposed structural dynamics at 0 ns (purple) and 10 ns (teal) are shown for p50 apo-protein (B) and p50-compound **5** complex (c). The overlapped models for p50 apo-protein at 0 ns (pre-MDS) and p50-compound **5** complex at 10 ns (post-MDS) are also depicted (d)

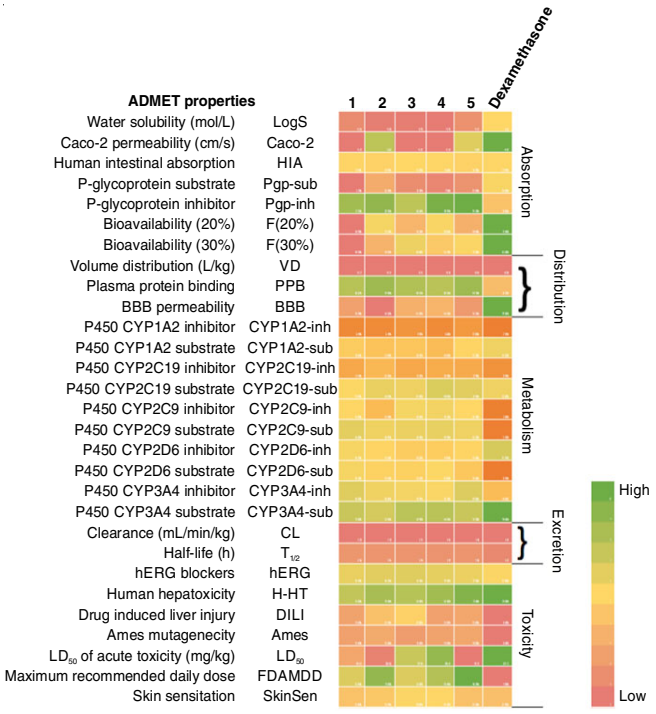

Fig. 7. ADMET prediction of the friedolanostanes identified in *Garcinia benthamii*

can lead to low to moderate oral bioavailability [34]. To increase the pharmacokinetics of these compounds, the mode of administration can be augmented *via* vectors or special drug delivery systems like nanomaterials. Recently, Kaps *et al.* [36] promoted that encapsulating low water-in soluble compounds like pentacyclic terpenes in a nanocarrier-delivery system would increase its bioavailability and overall pharmacokinetics properties. As a result, compounds **2-5**, having lower binding scores than dexamethasone, should nevertheless be given due consideration as promising phytochemicals based on their accrued ADMET measurements.

Conclusion

Through chemical investigation, five of the compounds obtained from dichloromethane extract of *G. benthamii* were identified to be friedolanostanes which three of them are newly reported compounds. Among all, two of the newly reported friedolanostane do exhibit a promising binding affinity (-4.1 kcal/mol) to p50 subunit as compared to marketed-drug dexamethasone (-3.7 kcal/mol). To further examine the druggability of the compounds, these friedolanostanes were subjected to ADMET analysis. In which, friedolanostanes may be a cytochromeP450 inhibitor and plasma protein binder that enhance its bioavailability and distribution. Yet, the cholesterol-like backbone of friedolanostanes does limit its water solubility and permeability, which can be further improved by drug-delivery system. Still, this study does propose a potential direction of friedolanostanes as a natural occurring p50 subunit inhibitor and act as potential anti-inflammatory agent and other p50-related diseases through *in silico* analysis. Further investigation can focus on studies like the structure-activity relationship or synthetic pathway for the most promising friedolanostane as an anti-inflammatory agent.

ACKNOWLEDGEMENTS

The authors acknowledge and dedicate this work, which could not have been achieved without Late Prof. Consolacion Y. Ragasa's guidance and contribution. A research grant from the De La Salle University Science Foundation through the URCO is gratefully acknowledged.

CONFLICT OF INTEREST

The authors declare that there is no conflict of interests regarding the publication of this article.

REFERENCES

1. R.E. Coronel, Important and Underutilized Edible Fruits of the Philippines, UPLBFI and DA-BAR (2011).
2. R.R. Lerom, *J. Nat. Stud.*, **6**, 49 (2007).
3. R.R. Lerom, *J. Nat. Stud.*, **3**, 27 (2004).
4. P.P. Goltenboth and F. Milan, A Guide to the Ecosystems of Palawan, Philippines, VISCA-GTZ Applied Tropical Ecology Program, Times Edition, Singapore (1998).
5. B. Elya, H.P. He, S. Kosela, M. Hanafi and X.J. Hao, *Nat. Prod. Res.*, **20**, 1059 (2006); https://doi.org/10.1080/14786410500462512
6. P. Amelia, B. Elya and M. Hanafi, *Int. J. Pharm. Tech. Res.*, **7**, 254 (2015).
7. J.M. Joseph and T. Supinya, *Afr. J. Biotechnol.*, **9**, 1848 (2010); https://doi.org/10.5897/AJB10.660
8. D.A. Bui, M.K. Vu, H.D. Nguyen, L.-T.T. Nguyen, S.V. Dang and L.-H.D. Nguyen, *Phytochem. Lett.*, **10**, 123 (2014); https://doi.org/10.1016/j.phytol.2014.08.019
9. M.T. de Santana Souza, J.R. Almeida, A.A. de Souza Araujo, M.C. Duarte, D.P. Gelain, J.C. Moreira, M.R. dos Santos and L.J. Quintans-Júnior, *Basic Clin. Pharmacol. Toxicol.*, **115**, 244 (2014); https://doi.org/10.1111/bcpt.12221
10. V.R. Yadav, S. Prasad, B. Sung, R. Kannappan and B.B. Aggarwal, *Toxins*, **2**, 2428 (2010); https://doi.org/10.3390/toxins2102428
11. Z.P. Wang, S.X. Cai, D.H. Liu, X. Xu and H. Liang, *Acta Pharmacol. Sin.*, **27**, 1474 (2006); https://doi.org/10.1111/j.1745-7254.2006.00442.x
12. O. Trott and A.J. Olson, *J. Comput. Chem.*, **31**, 455 (2010); https://doi.org/10.1002/jcc.21334
13. D. Schneidman-Duhovny, O. Dror, Y. Inbar, R. Nussinov and H.J. Wolfson, *Nucleic Acids Res.*, **36(Web server)**, W223 (2008); https://doi.org/10.1093/nar/gkn187
14. J. Dong, N.N. Wang, Z.J. Yao, L. Zhang, Y, Cheng, D, Ouyang, A,-P, Lu and D.-S. Cao, *J. Cheminform.*, **10**, 29 (2018); https://doi.org/10.1186/s13321-018-0283-x
15. ACD/ChemSketch, version 2010.2.26; Advanced Chemistry Development, Inc.: O.N. Toronto, Canada (2010).
16. Discovery Studio Visualizer, version 21.1.0.20298; Dassault Systèmes Biovia Corp: France (2020).
17. R.J. Anderson, Z. Weng, R.K. Campbell and X. Jiang, *Proteins*, **60**, 679 (2005); https://doi.org/10.1002/prot.20530
18. I.W. Davis, A. Leaver-Fay, V.B. Chen, J.N. Block, G.J. Kapral, X. Wang, L.W. Murray, W.B. Arendall, J. Snoeyink, J.S. Richardson and D.C. Richardson, *Nucleic Acids Res.*, **35(Web Server)**, W375 (2007); https://doi.org/10.1093/nar/gkm216
19. A. Kuriata, A.M. Gierut, T. Oleniecki, M.P. Ciemny, A. Kolinski and M. Kurcinski, *Nucleic Acids Res.*, **46(W1)**, W338 (2018); https://doi.org/10.1093/nar/gky356
20. N.M. O'Boyle, M. Banck, C.A. James and C. Morley, *J. Cheminform.*, **3**, 33 (2011); https://doi.org/10.1186/1758-2946-3-33
21. B. Bienfait and P. Ertl, *J. Cheminform.*, **5**, 24 (2013); https://doi.org/10.1186/1758-2946-5-24
22. V. Rukachaisirikul, A. Adair, P. Dampawan, W.C. Taylor and P.C. Turner, *Phytochemistry*, **55**, 183 (2000); https://doi.org/10.1016/S0031-9422(00)00191-6
23. H.D. Nguyen, B.T.D. Trinh, Q.N. Tran, H.D. Nguyen, H.D. Pham, P.E. Hansen, F. Duus, J.D. Connolly and L.H.D. Nguyen, *Phytochemistry*, **72**, 290 (2011); https://doi.org/10.1016/j.phytochem.2010.11.016
24. C.Y. Ragasa, M.C.S. Tan, D. Fortin and C.C. Shen, *J. Appl. Pharm. Sci.*, **5**, 62 (2015); https://doi.org/10.7324/JAPS.2015.50912
25. C.Y. Ragasa, O.B. Torres, J.M.P. Gutierrez, H.P.B.C. Kristiansen and C.C. Shen, *J. Appl. Pharm. Sci.*, **5**, 94 (2015); https://doi.org/10.7324/JAPS.2015.50416
26. C.Y. Ragasa, D.L. Espineli, E.M. Agoo and R.S. del Fierro, *Chin. J. Nat. Med.*, **11**, 264 (2013).
27. C.Y. Ragasa, V.A.S. Ng, V. Ebajo Jr, D. Fortin, M.M. De Los Reyes and C.C. Shen, *Der Pharm. Lett.*, **6**, 453 (2015).
28. C.Y. Ragasa, V.A.S. Ng, M.M. De Los Reyes, E.H. Mandia, G.G. Oyong and C.C. Shen, *Der Pharma Chem.*, **6**, 182 (2014).
29. J.M.C. Cayme and C.Y. Ragasa, *Kimika*, **20**, 5 (2004); https://doi.org/10.26534/kimika.v20i1.5-12
30. C.Y. Ragasa and J. de Jesus, *Res. J. Pharm. Biol. Chem. Sci.*, **5**, 701 (2014).
31. E. Arnold, D.M. Himmel and M.G. Rossmann, International Tables for Crystallography: Crystallography of Biological Macromolecules, John Wiley & Sons: Chichester, U.K., edn. 1, vol. F, pp. 520-525 (2001).
32. D. Eisenberg, R. Lüthy and J.U. Bowie, *Methods Enzymol.*, **277**, 396 (1997); https://doi.org/10.1016/S0076-6879(97)77022-8
33. A. Messaoudi, H. Belguith and J. Ben Hamida, *Theor. Biol. Med. Model.*, **10**, 22 (2013); https://doi.org/10.1186/1742-4682-10-22
34. B.C. Doak, B. Over, F. Giordanetto and J. Kihlberg, *Chem. Biol.*, **21**, 1115 (2014); https://doi.org/10.1016/j.chembiol.2014.08.013
35. M. Varma, *Pharmacol. Res.*, **48**, 347 (2003); https://doi.org/10.1016/S1043-6618(03)00158-0
36. A. Kaps, P. Gwiazdoñ and E. Chodurek, *Molecules*, **26**, 1764 (2021); https://doi.org/10.3390/molecules26061764